Investigating the Potential of Miniaturized Electrodynamic Tethers to Enhance ChipSats

IEPC-2013-373

Presented at the 33rd International Electric Propulsion Conference,
The George Washington University • Washington, D.C. • USA
October 6 – 10, 2013

Iverson C. Bell, III[1], Brian E. Gilchrist[2], David Liaw[3], Vritika Singh[4] and Kyle A. Hagen[5]
The University of Michigan, Ann Arbor, MI 48109, USA

and

Sven G. Bilén[6] and Jesse K. McTernan[7]
The Pennsylvania State University, University Park, PA 16802, USA

The sub-kilogram, "smartphone"-sized satellite is the next frontier in satellite miniaturization. The concept represents an evolution beyond the nanosatellite (1–10 kg) platform, made especially feasible by advances in sophisticated, low-power microelectronics. The result is that highly capable, cost-effective ultra-small satellites ("satellite-on-a-chip" or "ChipSat") as well as "constellations" of spacecraft for simultaneous, multipoint measurements show potential to perform meaningful science and other missions. However, "fleets" of ChipSats will need a high level of coordination and maneuvering capability (i.e., propulsion). Previous studies have found that short (few meters), semi-rigid electrodynamic tethers can provide 10-g to 1-kg satellites with complete drag cancellation and the ability to change orbit. Electron emitting and collecting plasma contactors are critical because they close the tether circuit in the ambient plasma, allowing current to be conducted in the tether. Our goal in this paper is to improve our current collection estimate by presenting progress made on ground-based plasma experiments that attempt to capture key characteristics of the LEO–tether system interaction, like the current collector's geometry and the ratio of the Debye length to the collector's characteristic dimensions. The paper will also present progress toward an in-space experiment that will demonstrate miniature tether technology.

Nomenclature

B	=	[T] magnetic field flux density
$\mathbf{B}$	=	[T] magnetic field flux density, represented as a vector
$\mathbf{F}_{\text{Lorentz}}$	=	[N] Lorentz force
I_{anode}	=	[A] anode electron collection current
I_e	=	[A] probe electron current
I_i	=	[A] probe ion current

[1] Ph.D. Candidate, Electrical Engineering, 1301 Beal Ave., icbell@umich.edu.
[2] Professor, Electrical Engineering and Space Science, 1301 Beal Ave., brian.gilchrist@umich.edu.
[3] Ph.D. Candidate, Electrical Engineering, 1301 Beal Ave., liawd@umich.edu.
[4] Graduate Student, Space Engineering, 2455 Hayward St., singhv@umich.edu.
[5] Graduate Student, Space Engineering, 2455 Hayward St., kyleha@umich.edu.
[6] Assoc. Professor, Engineering Design, Electrical Engineering, and Aerospace Engineering, 213 Hammond Bldg., SBilen@engr.psu.edu.
[7] Ph.D. Candidate, Aerospace Engineering, 304 Electrical Engineering East Bldg., jkm249@psu.edu.

I_{OML} = [A] orbital-motion-limited current
I_{PM} = [A] Parker–Murphy current
I_{probe} = [A] probe current
I_{tether} = [A] tether current
$I_{thermal}$ = [A] thermal current
$I_{TSS\text{-}1R}$ = [A] TSS-1R modified Parker–Murphy current
I_{WLP} = [A] current collected by the wide sweeping Langmuir probe on Floating Potential Measurement suite
k = [J·K^{-1}] Boltzmann constant
L = [m] tether length
$\mathbf{L}$ = [m] tether length, represented as a vector
m_e = [kg] mass of electron
n_e = [m^{-3}] electron density
n_g = [m^{-3}] neutral density
n_i = [m^{-3}] ion density
q = [C] charge of an electron
r_p = [m] probe radius
r_L = [m] Larmor radius or gyroradius
r_{sheath} = [m] sheath radius
T_e = [K] electron temperature
$v_\perp$ = [m·s^{-1}] component of electron velocity perpendicular to the magnetic field
v_{the} = [m·s^{-1}] the thermal speed of electrons
v_{thi} = [m·s^{-1}] the thermal speed of ions
v_{ths} = [m·s^{-1}] the speed of the spacecraft
V_{anode} = [V] anode voltage
V_{gate} = [V] cathode base-gate voltage
V_{probe} = [V] probe voltage
α = [2.5] constant
β = [0.5–1] constant, varying with anode geometry
ε_0 = [F·m^{-1}] permittivity of free space
λ_D = [m] Debye length
λ_{MFP} = [m] mean free path for ion-neutral charge exchange collisions
σ_{Xe} = [m^2] xenon charge exchange collision cross section
φ_0 = [V] intermediate potential
φ_f = [V] floating potential
φ_p = [V] plasma potential
ω_{ce} = [rad·s^{-1}] electron cyclotron frequency

I. Introduction

The sub-kilogram, "smartphone"-sized satellite is the next frontier in satellite miniaturization. The concept represents an evolution beyond the nanosatellite (1–10 kg) platform, made possible because of advances in electronics miniaturization and power reduction. These small sensor spacecrafts, known as picosatellites (100 g–1 kg) and femtosatellites (<100 g), have longest dimensions that range from tens of centimeters down to a few centimeters in length.[1–4] This architecture can be thought of as a "satellite-on-a-chip," or ChipSat. Due to their small size and mass, ChipSats show potential to be dramatically less expensive (on a per unit basis) to boost into orbit.[1] As a result, it may be possible to launch large numbers of these satellites, unlocking the potential for low cost constellations. Reconfigurable, adaptable fleets may be capable of multipoint, simultaneous measurements; rapid re-measurement of a single location; unique multipoint remote sensing; and unique multipoint *in situ* measurements. Applications include using fleets for global monitoring of natural disasters or, alternatively, enhancing space weather modeling via multi-point measurements.[5,6]

The most capable constellations of ChipSats, however, will likely need a high level of coordination and maneuverability, and this will demand propulsion. Flat ChipSats also can have an inherently high area-to-mass ratio, resulting in a short lifetime in low Earth orbit (LEO) due to atmospheric drag. A propulsion system would be needed to extend the mission lifetime of these satellites. While a satellite using chemical propulsion with proper attitude pointing can maintain altitude, the required propellant volume will increase with the satellite's intended lifetime.

Thus, the use of a traditional thruster with propellant and directed flow to compensate for drag and possibly for maneuverability would significantly increase the size, mass, and complexity of femtosatellites.

Previous trade studies have shown that a short (few meters), semi-rigid electrodynamic tether has the potential to provide propellantless propulsion for ultra-small satellites.[7,8] The tether can also potentially enhance communication as an antenna. An illustration of the concept is shown in Fig. 1.

An electrodynamic tether's propulsive force scales with tether current. In previous studies, thrust estimates were based on a set of simplifying assumptions made to facilitate estimating tether current. In this paper, we revisit these assumptions and describe a ground-based laboratory experiment in which we simulate characteristics of the orbital environment in order to refine previous current estimates. We also share developments in the Miniature Tether Electrodynamics Experiment (MiTEE) mission being planned to demonstrate the miniature tether concept.

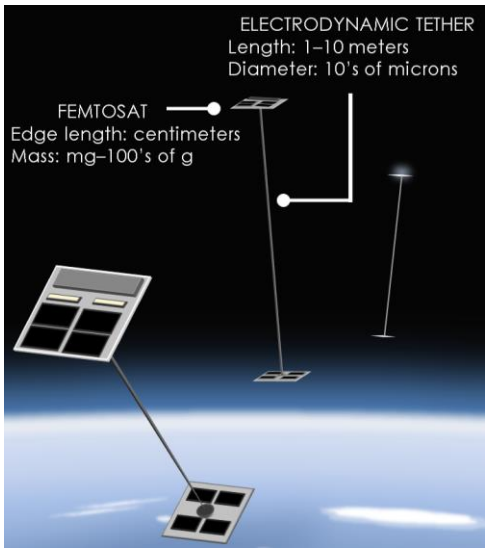

Figure 1. An illustration showing the concept of ED tethers connecting pairs of femtosatellites in a maneuverable, coordinated fleet.[7]

II. Background

A. Electrodynamic Tether Background

An electrodynamic tether (ED tether) is a long conducting wire. The cable may by suspended from a spacecraft or, alternatively, connect a pair (or more) of spacecraft. Current conducted by the tether produces a propulsive force in the presence of a planetary magnetic field, given by

$$\mathbf{F}_{\text{Lorentz}} = \int_0^L I_{\text{tether}} d\mathbf{L} \times \mathbf{B}. \tag{1}$$

Current is collected at one end of the tether from the ambient ionospheric plasma and emitted back into the ionosphere at the opposite end. Current closure takes place in the ionosphere.

B. System Concept Description

In the proposed system concept, an insulated-but-conducting, semi-rigid tether ranging from 1–20 meters in length connects a pair of nearly identical ChipSats. Each of the satellites is equipped with power generation (solar panels), energy storage, electron emission, and electron collection capability. Figure 2 shows an illustration of the system concept. Although various satellite sizes have been considered in previous trade studies, here we highlight the 10 cm × 10 cm × 1.25 cm, 100-g satellite.

Efficient electron emission can be achieved through the use of a field emission array cathode (FEAC). For a typical FEAC, electrons are emitted from the "base," where there is a 2-D array of carbon nanotubes or micrometer-scale cones.[9,10] A positively biased grid, or "gate," near the base establishes an electric field (at the level of single $V \cdot nm^{-1}$) that induces quantum mechanical tunneling of electrons out of the emitter tips. Electrons travel through openings in the gate and into the ambient plasma. The emission current is controlled by adjusting the base-gate voltage, V_{gate}.

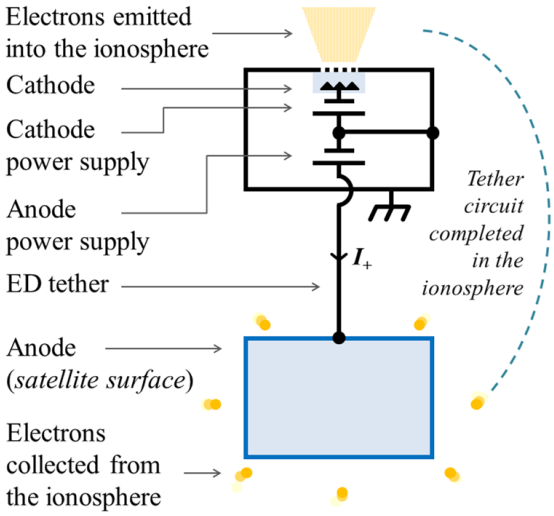

Figure 2. A diagram of the system concept. *The core components of the tether propulsion system are shown. In a possible alternative configuration, the anode and cathode power supplies would be located on separate satellites, though similarly connected.*

The satellite at the opposite end of the tether will act as the electron collecting anode. Conducting surfaces exposed to the ambient plasma can be positively biased to attract electrons. In order to increase the surface area for collection, a transparent conductor (like ITO) can be used to coat solar cells.[11]

Although there is a well characterized relationship between electron emission current and base-gate voltage for FEACs[12], the authors have not identified any models that predict the current collection capability of a positively biased ChipSat-sized, ChipSat-shaped conductor in LEO. A set of simplifying assumptions outlined in the following section were made to facilitate estimating the collection current.

III. Theoretical Approach to Estimating Anode Current

For over a century, theoretical models have been developed to describe the phenomenon of current collection to a conducting body in a plasma.[13,14] In this section, we provide a brief summary of relevant theories and assumptions made to estimate the current collection. A more comprehensive discussion is presented in Ref. 15.

A. Collection Current Models

When a positively biased electrode (anode) is inserted into a plasma, electrons are drawn to it and ions are repelled. As charged particles in the plasma redistribute, a non-neutral ($n_e > n_i$) region known as the sheath forms around the object that shields the undisturbed plasma from the potential disturbance. Although the potential difference is mostly screened out in the sheath, a small fraction of the total voltage falls in a second, extended region that connects the sheath to the plasma known as the pre-sheath. The characteristic length for electric field screening (exponentially decaying) is the Debye length, expressed as

$$\lambda_D = \sqrt{\frac{\varepsilon_0 k T_e}{q^2 n_e}}, \tag{2}$$

where the sheath is often assumed to extend several Debye lengths or more, depending on spacecraft potential with respect to the plasma potential.

If the sheath is large with respect to the electrode ($\lambda_D \geq r_p$), the orbital effects of particles that enter the sheath become significant. In a collisionless, non-drifiting, unmagnetized plasma where $\lambda_D \geq r_p$, orbital-motion-limited (OML) theory can be used to predict the collection current to simple electrode geometries (spheres, infinite cylinders, and infinite plates). If $V_{\text{anode}} > \varphi_p$ (e.g., collection in the electron saturation regime), the current is given by[16]

$$I_{\text{OML}} = I_{\text{thermal}} \left(1 + \frac{q\left(V_{\text{anode}} - \varphi_p\right)}{k T_e} \right)^{\beta}. \tag{3}$$

where $\beta = 1$ for a sphere, $\beta = 0.5$ for an infinite cylinder, and $\beta = 0$ for an infinite plate. The thermal current,

$$I_{\text{thermal}} = A_{\text{probe}} n_e q \sqrt{\frac{k T_e}{2\pi m_e}} \tag{4}$$

is the random thermal current collected at the edge of the sheath. The increase in current with applied voltage in Eq. (3) corresponds to an increase in the sheath size. If $\lambda_D << r_p$, the sheath is extremely thin and the resulting collection current is simply the thermal current incident at the satellite's surface.[17]

There is a magnetic field in LEO, however, and it impacts current collection. Magnetization violates an assumption of OML theory. Ignoring collisions and electric fields, electrons in LEO travel in a helical trajectory along magnetic field lines with a gyroradius given by

$$r_L = \frac{m_e v_\perp}{eB}. \tag{5}$$

If the electrode is large with respect to the gyroradius, the collection current at the sheath edge is limited to electrons traveling along intersecting magnetic flux tubes. Parker–Murphy provides the theoretical model for electron

collection by a large ($r_L << r_p$), positively biased sphere in a non-drifting, collisionless, magnetized plasma, given as[18]

$$I_{\mathrm{PM}} = \frac{I_{\mathrm{thermal}}}{2}\left(1+\left(\frac{V_{\mathrm{anode}}-\varphi_p}{\varphi_0}\right)^{1/2}\right) \tag{6}$$

where the intermediate potential φ_0 is given by

$$\varphi_0 = \frac{m_e {\omega_{\mathrm{ce}}}^2 r_p^2}{8q}. \tag{7}$$

The thermal current in Eq. (6) is divided by 2 because the collection area is $2\pi {r_p}^2$, or the 2-dimensional projection of the sphere perpendicular to the magnetic field.

The Parker–Murphy model was modified based on mission data from the Tether Satellite Systems Reflight (TSS-1R), which was theorized to be affected by the mesothermal plasma speeds experienced in orbit ($v_{\mathrm{thi}} < v_{\mathrm{sat}} < v_{\mathrm{the}}$), giving the expression[19]

$$I_{\mathrm{TSS\text{-}1R}} = \alpha\frac{I_{\mathrm{thermal}}}{2}\left(1+\left(\frac{V_{\mathrm{anode}}-\varphi_p}{\varphi_0}\right)^{\beta}\right) \tag{8}$$

where, based on the TSS-1R mission results, average values for β and α can be estimated as: $\beta \approx 0.5$ and $\alpha \approx 2.5$. Mesothermal plasma speed is important because it causes significant sheath asymmetry and possibly instability (e.g., turbulent electron scattering) that affects current collection.[20–22]

B. Challenges Associated with Estimating Anode Current

Estimating the current collected to the surface of a ChipSat is made complex for several reasons. The authors are aware of no theory that captures the effects of plasma flow for an electrode that has non-standard geometry and whose characteristic dimension is on par with the Debye length and the gyroradius. One of the assumptions of the Parker–Murphy model (and its TSS-1R modified version) is that the gyroradius is small relative to the collector size. In the region of LEO we have considered in this trade study, the average electron gyroradius is approximately 3 cm. The TSS-1R anode had a radius of 80 cm. The satellite considered in this trade study has an equivalent radius of 5 cm (and more generally we consider pico- and femtosats that are even smaller). Thus, direct application of the TSS-1R modified Parker–Murphy model is suspect. In addition, the possible cuboid shape of the pico- and femtosat further complicates predicting current. Many of the proposed ChipSat designs are generally planar and rectangular because components are mounted on printed circuit boards (PCBs) and/or silicon wafers. The Parker–Murphy and TSS-1R modified Parker–Murphy models are only defined for conducting spheres while OML theory is defined for spheres, infinite cylinders, and infinite plates. Experiments have been conducted to better understand the current collection behavior of similarly shaped electrodes in a flowing plasma, but the electrode sizes relative to the Debye length were large compared to our electrodes.[23]

C. Simplifying Assumptions Made to Facilitate Estimating Anode Current

For a probe in an unmagnetized, non-drifting plasma, the sheath surrounding the probe will expand outwards with increasing bias voltage. If the sheath is very large with respect to the probe, it may mask the details of the probe's shape. We have therefore assumed that at high potentials, the cuboid-shaped satellite collects current *approximately* like a sphere with a diameter equal to the satellite's longest edge. The equivalent radius of the 10 cm × 10 cm × 1.25 cm ChipSat would be 5 cm.

In order to make a rough estimate of the sheath size, we reason that the current collected by a positively biased conductor must equal the net current passing through the outer edge of the sheath boundary (i.e., no ion generation or secondary electron emission). For our application, it is also safe to assume that the potential difference between the conducting body and the undisturbed ambient plasma is much larger than the electron temperature, T_e, and falls across the sheath (any pre-sheath potential is ignored here). We also assume that the entire ChipSat's surface is

conducting and capable of collecting current. Since the electron thermal current at the sheath edge is equal to the current collected by the probe, given by Eq. (3), we solve for a rough approximation of the sheath radius, giving[24]

$$r_{\text{sheath}} = r_p \sqrt{1 + \frac{q\left(V_{\text{probe}} - \varphi_p\right)}{kT_e}}\,. \tag{9}$$

For a sphere in a 0.1-eV-temperature plasma charged to 100 volts above the plasma potential, the estimated sheath radius is approximately 30 times the probe radius.

A second, more conservative estimate for sheath thickness was developed empirically for conducting spheres in stationary, non-magnetized Maxwellian plasmas. The estimated sheath radius is[25]

$$r_{\text{sheath}} = 0.83 r_p^{1/3} \lambda_D^{2/3} \sqrt{\frac{qV_{\text{probe}}}{kT_e}}\,. \tag{10}$$

For a 5-cm-diameter sphere at 100 V in a 0.1-eV plasma with density ranging from 10^{10}–10^{12} m^{-3}, the sheath is estimated to be 17–80 cm thick, or 3.4–16 times the probe radius. In both scenarios, the large estimated sheath radius relative to the probe size helps justify using the spherical collector approximation. However, the thick sheath estimate is more appropriate when plasma densities are low because λ_D is larger. Additionally, the sheath radius could be smaller if turbulent electron scattering takes place.

After assuming a spherical collector, we chose to be conservative and utilized an expression developed by a research team to interpret plasma parameters from the Floating Potential Measurement Unit on the International Space Station. The Floating Potential Measurement Unit employed the wide sweeping Langmuir probe instrument (WLP), a sphere of 5 cm radius, to do current–voltage (I–V) sweeps from –20 V up to 80 V. The expression[26]

$$I_{\text{WLP}} = \frac{I_{\text{thermal}}}{2}\left(1 + \frac{q\left(V_{\text{anode}} - \varphi_p\right)}{kT_e}\right)^{\beta} \tag{11}$$

was then fit to current–voltage data in the electron saturation region with different values of the dimensionless parameter β. The values of β varied between 0.5 and 1, with an average during a 2-hour time window that appears to be approximately 0.8.[26] Here, we choose $\beta = 0.85$ for our model, which is close to the apparent average β value.

IV. Plasma Chamber Experiments

The purpose of this experiment is to improve our current collection estimate by conducting ground-based plasma experiments that capture key characteristics of the LEO-tether system interaction, including the plasma flow, the ChipSat geometry, and the ratio of the Debye length to the ChipSat characteristic dimensions. This paper is intended to be the first of many experiments, so we also comment on improvements that could be made for future experiments.

A. Experimental setup and methods

1. Vacuum facility and plasma source

The system consists of a vacuum chamber with a mechanical roughing pump and a cryogenic pump. The chamber is a stainless steel cylindrical tank that is approximately 1 m in diameter and 2 m in axial length. The corresponding volume inside the vacuum chamber is ~1.6 m^3. The cryogenic pump has a pumping speed of 2500 $\text{l}\cdot\text{s}^{-1}$ for argon. The chamber can maintain a base pressure of about 8×10^{-6} Torr.

A lanthanum hexaboride (LaB_6) hollow cathode was used to create a high-speed plasma. There are several examples of hollow cathodes being used to simulate spacecraft-plasma

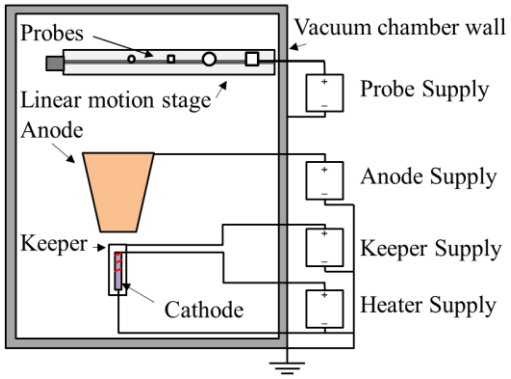

Figure 3. Setup of the vacuum chamber showing the hollow cathode plasma source and the probes.

interactions in ground-based laboratories.[27–29] The hollow cathode in our experiment was originally designed for hall thrusters and is capable of a 5–60 A discharge current. Other resources provide a detailed description of this cathode.[30,31] Xenon was used as the source gas for the hollow cathode because it is chemically inert and has a relatively low first ionization energy (~12.1 eV). The cathode flow rate was 5 sccm and the operating pressure during cathode flow was 2.6×10^{-5} Torr.

Prior to initiating the plasma discharge, the LaB_6 insert was heated by applying ~200 W to the heater coil. Next, a 100–V bias was applied to the cathode assembly's graphite keeper to initiate the discharge. After a faint purple glow was visible in the orifice and the keeper power supply detected current, the water-cooled, conical anode at the cathode exit plane was biased to 28.2 V to maintain the discharge. When the anode current reached 18.9 A and the plume appeared to be in a steady state, the heater power supply was turned off and the keeper was allowed to float. The electrical diagram is shown in Fig. 3. Images of the experimental apparatus are shown in Figs. 4–6. There was also a retarding potential analyzer located downstream from the cathode that was part of a different experiment.

Figure 4. Experimental setup.

2. Langmuir probes and test articles

Four probes were positioned about 90 centimeters downstream from the hollow cathode. The probes were mounted on a linear motion stage that was remotely controlled so each probe could take measurements in a single location. The probes were spaced 8.9 cm apart and distanced even further from the chamber walls. A Keithley 2400 SourceMeter was used to produce a 751-point voltage range sweep from –50 V to 100 V. The voltage resolution was 0.2 V.

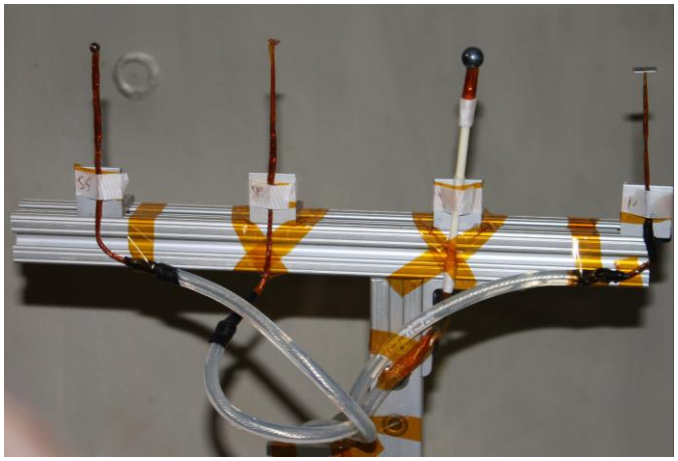

Figure 5. Probes mounted in the vacuum chamber. *From left to right, there is the 0.5-cm spherical probe, the 0.5-cm planar probe, the 1-cm spherical probe, and the 0.5-cm planar probe.*

Two of the probes were stainless steel, spherical Langmuir probes—a 1-cm diameter sphere and a 0.5-cm diameter sphere—that we used to determine plasma parameters such as electron density, electron temperature, and plasma potential. The larger sphere is referred to as the 1-cm spherical probe and the smaller one is referred to as the 0.5-cm spherical probe.

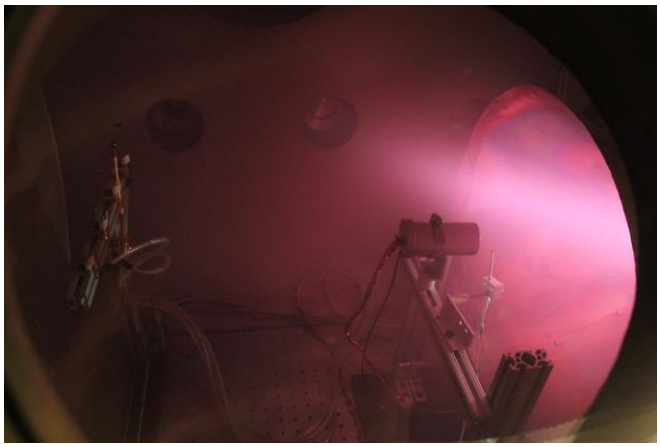

Figure 6. The probes in the high speed plasma plume.

Previously, we assumed that the ChipSat would collect current like a sphere with an equivalent diameter equal to the satellite's longest edge, so the ChipSat-shaped probes were chosen to have edge lengths equal to the spherical probes' diameters. The dimensions for the probes were 1 cm × 1 cm × 0.05 cm and 0.5 cm × 0.5 cm × 0.062 cm. The larger ChipSat-shaped probe is referred to as the 1-cm planar probe and the smaller one is referred to as the 0.5-cm planar probe. The 1-cm planar probe was made from tungsten and the 0.5-cm planar probe was made from copper.

The dimensions of the 1-cm and 0.5-cm planar probes were also chosen to be (approximately) representative, after scaling, of a current collecting ChipSat in the ionosphere. It is well understood that the shape of a conducting body in a plasma and the size of the body relative to the Debye length are important for determining the I–V characteristic.[32] Both of these factors influence the shape and the size of the sheath, which, in turn, impact current collection. In this experiment, we aimed to design planar test probes that would approximate the shape and size of the anode relative to the Debye length. We approximated the size of the anode to the Debye length by scaling the dimensions of the planar probe with respect to the Debye length.

In LEO, we expect a 0.1-eV to 0.2-eV plasma with an electron density ranging from 10^{10} m^{-3} to 10^{12} m^{-3}.[32] The corresponding Debye length is 0.2–3.3 cm. Thus, the 10-cm edge of the ChipSat that is the focus of this paper would be 3–42 times the Deybe length. In preliminary tests, we calculated that the Debye length in the laboratory facility would be about 1 mm. We chose to design one planar probe so the longest edge would be 5 times the Debye length and another so the longest edge would be 10 times the Debye length, resulting in one 0.5-cm planar probe and one 1-cm planar probe. The 1-cm planar probe could be more representative of a ChipSat in a low density, large Debye length region of the ionosphere and the 0.5-cm planar probe could be representative of a ChipSat in a higher density, lower Debye length region of the ionosphere.

The test probe design, however, is not ideal. Although the 0.5-cm planar probe edge length was half of the 1-cm planar probe edge length, the height of the 0.5-cm probe length was not similarly scaled. In addition, the planar probes were made from different materials, and this can impact collection as well. Even with these nonidealities, we believe the probes can provide insight into the current collection characteristic of a ChipSat in different Debye length regimes.

3. Assessing the impact of charge exchange collisions on the plasma flow

One goal of the experiment was to simulate current collection in a flowing plasma. We positioned the probes in the far field of the cathode plume to ensure that the Debye length was ~1 mm. Expecting the electron temperature to be a few eV downstream of the hollow cathode plume, we desired a plasma density between 1×10^{13} m^{-3} and 1×10^{14} m^{-3} to ensure that the Debye length is the appropriate range. Although the plasma at the cathode orifice will be orders of magnitude denser than this,[30] the hollow cathode plume expands after it exits the cathode and the plasma density decreases significantly with distance.[33]

The probes cannot be too far from the hollow cathode, however, because charge exchange collisions will reduce plasma flow effects. Charge exchange collisions can transform a streaming plasma into a population of slow moving ions (at neutral temperature). Thus, this plasma would not represent the mesothermal plasma seen by an orbiting spacecraft. As an ion travels through a neutral background gas, the probability of a charge exchange collision increases with distance. The mean free path, or the average distance traveled before a collision takes place, can be calculated as

$$\lambda_{\mathrm{MFP}} = \frac{1}{n_g \sigma_{\mathrm{Xe}}}. \tag{12}$$

The neutral density during the experiment was 8.57×10^{17} m^{-3}. The charge transfer collision cross section between Xe and Xe^+ is approximately 8.3×10^{-19} m^2 for 1–5 eV xenon ions.[34,35] Using Eq. (12), the mean free path was about 1.4 m. We then used the Beer–Lambert law to estimate that only ~52% of the ions had not undergone a charge exchange collision at 90-cm distance from the cathode, which is where the probes were located. The result is that 48% of the ions make up a thermalized, non-drifting background population. So, although the plasma was streaming, it was not an ideal high speed flowing plasma. Additional diagnostic techniques would be needed to calculate the plasma flow velocity.

B. Results

The Langmuir probe data are shown in Fig. 7.

1. Parts of the I–V characteristic

The measured probe current is the sum of the electron and ion currents, or $I_{\mathrm{probe}} = I_e + I_i$. By convention, positive current denotes a net collection of electron current.

At the plasma potential, the probe collects thermal current from the plasma, which is expressed in Eq. (4). When the potential applied to the probe V_{probe} is below the plasma potential, a sheath forms around the probe that repels electrons in the plasma. The potential energy barrier for electrons increases as the probe bias becomes more negative. As a result, the electron current decreases exponentially with probe voltage. The region of exponential current decay is called the electron retardation region.

The measured current decreases to zero (I_{probe} = 0) when the electron and ion currents are equal. The voltage at I_{probe} = 0 is referred to as the floating potential. When the potential applied to the probe is set below the floating potential, the electron current continues to decrease and $I_{probe} = I_i$. This region of the I–V characteristic is called the ion saturation region. The ion saturation current is (nearly) constant with applied probe voltage. Reference 36 provides a more thorough discussion about the regions of the Langmuir probe sweep.

2. Langmuir probe analysis

The floating potential is simply taken as the potential where I_{probe} = 0. The electron temperature and density can be deduced from the electron current. We calculate the electron current by subtracting the ion saturation current from the probe current. In the electron retardation region, the slope of $\ln(I_e) - V_{probe}$ plot gives the inverse of the electron temperature in eV, or q/kT_e. The plasma potential can be obtained from the intersection of lines fit to the electron retardation and saturations regions of $\ln(I_e) - V_{probe}$ plot.[36] The graph of the $\ln(I_e) - V_{probe}$ characteristic as well as the lines fit to the electron retardation and saturation regimes is shown in Fig. 8.

The plasma parameters are provided in Table 1. The values derived from the 0.5-cm spherical probe and the 1-cm spherical probe are in agreement. The Debye length is about 1 mm, which accomplishes our goal of generating a plasma environment in which the Debye length is the same size scale as the largest ChipSat dimension. The most significant discrepancy is the plasma potential. Repeat measurements were not taken by each probe in a single location, so it is not clear if the plasma parameters actually varied between probe measurements or if this simply indicates error in the probe measurement.

In future experiments, an emissive probe could be used to provide a more accurate measurement of the plasma potential. It will

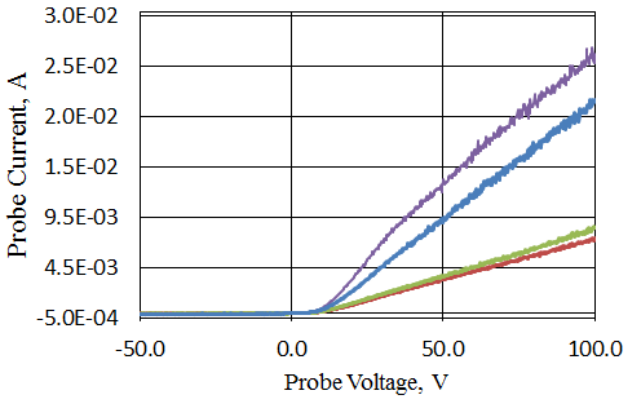

Figure 7. The current-voltage characteristic for each type of probe. *The characteristics for the 1-cm spherical probe (purple), the 1-cm planar probe (blue), the 0.5-cm spherical probe (red), the 0.5-cm planar probe (green).*

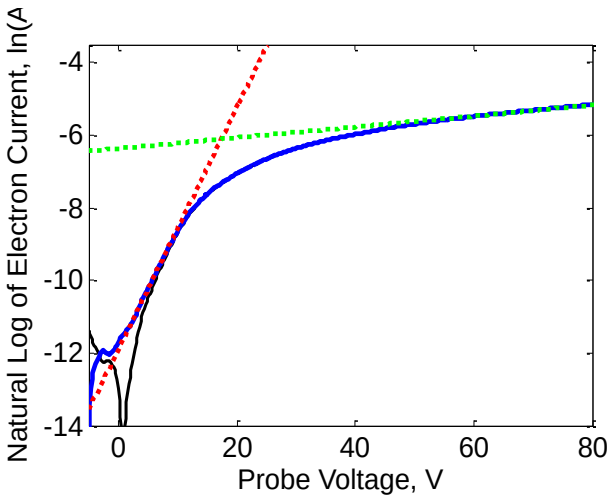

Figure 8. The $\ln(I_e)$–V characteristic for the 0.5-cm spherical probe. *The natural log of the probe current is shown in black. The electron current (ions subtracted) is shown in blue. The red line is the best fit line for the electron retardation region and the green line is the best fit line for the electron saturation region.*

Table 1. Plasma parameters 0.9 m down-stream from the source.

Parameters	Values from the 1-cm Spherical Probe	Values from the 0.5-cm Spherical Probe	Units
φ_f	-0.2	0	V
φ_p	19.4	17.4	V
kT_e/q	3.3	3.0	eV
n_e	1.1×10^{14}	1.3×10^{14}	m^{-3}
λ_D	1.3×10^{-3}	1.1×10^{-3}	m

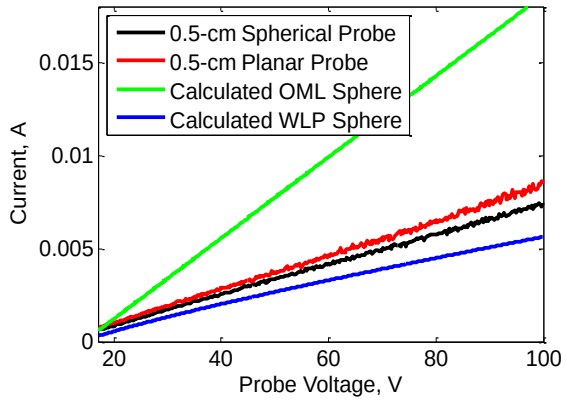

Figure 9. The I–V characteristic for the 0.5-cm spherical probe and the 0.5-cm planar probe compared to current calculated by the OML and WLP models.

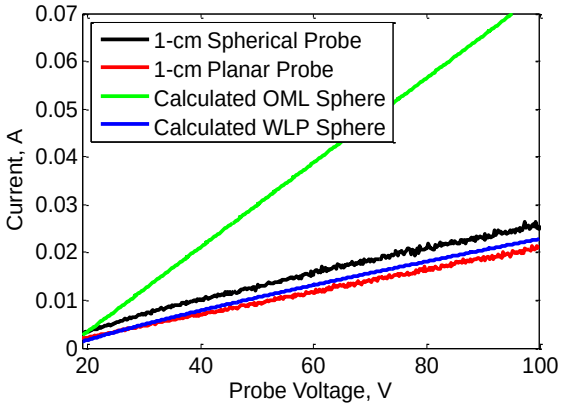

Figure 10. The I–V characteristic for the 1-cm spherical probe and the 1-cm planar probe compared to current calculated by the OML and WLP models.

also be important to do more I–V sweeps in each position to observe changes in the plasma properties over time. Finally, we can also consider deducing plasma parameters from the planar probes.

3. Analysis of the ChipSat-shaped probes

In this section, we address the current collection behavior of the ChipSat-shaped planar probes. The comparison of the planar and the spherical probes is shown in Figs. 9 and 10. We are interested in collecting current in the electron saturation regime, so only voltages above the plasma potential are shown.

All of the current measurements are below the OML predicted current. The Debye length is neither the same size nor larger than any of the probes tested, so the OML theory for thick sheaths cannot readily be applied. There were no magnetic field measurements taken inside the vacuum chamber, so we were unable to compare the collection currents to the Parker–Muphy or TSS-1R modified Parker–Murphy currents. However, as those expressions are better suited for current-collecting spheres that are large with respect to the gyroradius, we do not expect the expressions to accurately predict the collection current. It will be important in future experiments to analyze the role of magnetic field effects in influencing electron current collection.

The planar probes' current collection behavior is somewhat similar to that of the spherical probes, although there are some noticeable differences. The 0.5-cm planar probe current is slightly higher than the 0.5-cm spherical probe current. Although it is not clear why, we believe there may be large electric fields at the probe's edges and corners, and this enhances current collection. However, the 1-cm planar probe, which also has edges and corners, collects *less* current than the 1-cm spherical probe. Additional experiments and simulations would be needed to better explain the behavior of both probes.

Additionally, the planar probe current collection characteristics can be compared to the current predicted by the WLP model. In the voltage range tested, the WLP model underpredicts the collection current to the 0.5-cm planar probe by about 30% and overpredicts the collection current to the 1-cm planar probe by 10–15%. Thus, based on this limited data set, we believe the WLP model provides a reasonable estimate for collection current.

Our ability to draw conclusions about the current collection behavior of the planar probes from this voltage range is limited with the current data set. The maximum voltage is only $23kT_e/q$ above the plasma potential. This translates into a few volts in LEO, where the electron temperature is in the 0.1–0.2 eV range. We limited the maximum voltage in the I–V sweep to 100 V to prevent the probe current from becoming a significant fraction of the anode current and impacting the hollow cathode. However, the anode current is several hundred times larger than the probe current, so we believe higher probe voltages can be used in future experiments without compromising the hollow cathode operation.

V. MiTEE Mission

An in-orbit experiment is being planned by students at the University of Michigan to demonstrate the femtosat ED tether concept in the LEO environment. The Miniature Tether Electrodynamics Experiment (MiTEE) mission is a technology demonstration mission that will utilize CubeSat capabilities to deploy a ChipSat-tether system and assess the key dynamics and electrodynamics fundamental to the system's successful operation. The central questions motivating the mission include: (I) (Primary) Can the miniature tether provide stable, practical thrust for drag make-up and basic propulsion for "smart phone" sized ChipSats? (II) (Secondary) Can the miniature tether and pico/femtosatellite system serve in other roles? This could include, among others, that the miniature tether could be the basis for a useful, enhanced antenna for communication with the ground. An illustration of the system concept is shown in Fig. 11.

Figure 11. MiTEE mission spacecraft concept showing the CubeSat deploying the endmass. *Here, the tether is only deployed a short distance.*

VI. Summary

The purpose of the work reported here is to improve our current collection estimate by conducting ground-based plasma experiments that capture key characteristics of the LEO-tether system interaction. Although we captured some characteristics, like the ChipSat geometry and the ratio of the Debye length to the ChipSat characteristic dimensions, there is still a need to (i) consider additional plasma diagnostic techniques, (ii) investigate the current collection behavior for alternative ChipSat shapes and sizes, (iii) test the probes in higher voltages, (iv) analyze the impact of magnetic field effects on our probes, and (v) study how the planar probes could be used to deduce plasma parameters. Nevertheless, this facility seems to be well suited for future experiments. Furthermore, the experiment appears to have indicated that an existing model can be used to make rough estimates of the collection current characteristic of a planar anode. Additional laboratory tests are being planned to help us understand this more.

Acknowledgments

The authors gratefully acknowledge support from AFOSR grant FA9550-09-1-0646, the National Science Foundation Graduate Student Research Fellowship under Grant No. DGE 1256260, and the Michigan Space Grant Consortium. I. C. Bell would also like to thank K. Trent for providing knowledge and laboratory training, ElectroDynamic Applications, Inc. for use of their vacuum facilities, and the support of the Plasmadynamics and Electric Propulsion Laboratory (PEPL), Director Prof. Alec Gallimore.

References

[1] Barnhart, D. J., Vladimirova, T., Baker, A. M., and Sweeting, M. N., "A low-cost femtosatellite to enable distributed space missions," *Acta Astronautica*, vol. 64, Jun. 2009, pp. 1123–1143.

[2] Barnhart, D., Vladimirova, T., Sweeting, M., Balthazor, R., Enloe, L., Krause, H., Lawrence, T., Mcharg, M., Lyke, J., White, J., and Baker, A., "Enabling Space Sensor Networks with PCBSat," *AIAA/USU Conference on Small Satellites*, Aug. 2007.

[3] Janson, S., and Barnhart, D., "The Next Little Thing: Femtosatellites," *AIAA/USU Conference on Small Satellites*, Aug. 2013.

[4] Barnhart, D. J., Vladimirova, T., and Sweeting, M. N., "Very-Small-Satellite Design for Distributed Space Missions," *Journal of Spacecraft and Rockets*, vol. 44, Nov. 2007, pp. 1294–1306.

[5] Bouwmeester, J., and Guo, J., "Survey of worldwide pico- and nanosatellite missions, distributions and subsystem technology," *Acta Astronautica*, vol. 67, Oct. 2010, pp. 854–862.

[6] P. P. Sundaramoorthy, E. G., "Systematic identification of applications for a cluster of femto-satellites."

[7] Bell, I., Gilchrist, B., Liaw, D., Singh, V., Hagen, K., Lu, C., Cutler, J., Bilén, S., and McTernan, J., "Investigating the Feasibility and Mission Enabling Potential of Miniaturized Electrodynamic Tethers for Femtosatellites and Other Ultra-small Satellites," *AIAA/USU Conference on Small Satellites*, Aug. 2013.

[8] Bell, I., Gilchrist, B., Bilén, S., and McTernan, J., "Investigating the Use of Miniaturized Electrodynamic Tethers to Enhance the Capabilities of Femtosatellites and other Ultra-small Satellites," *AIAA/USU Conference on Small Satellites*, Aug. 2012.
[9] Yasushi Okawa, S. K., "An experimental study on carbon nanotube cathodes for electrodynamic tether propulsion," *Acta Astronautica*, 2007, pp. 989–994.
[10] Anguero, V. M., and `Adamo, R. C., "Space Applications of Spindt Cathode Field Emission Arrays," *6th Spacecraft Charging Technology*, 1998, pp. 347–352.
[11] McTernan, J. K., Bilén, S. G., Bell, I. C., and Gilchrist, B. E., "Current Collection to the Plasma Interaction with Femtosatellite- and Cubesat-Scale Electrodynamic Tether Subsystems," *AIAA Space 2012 Conference*, Pasadena, CA: 2012.
[12] Whaley, D. R., Duggal, R., Armstrong, C. M., Bellew, C. L., Holland, C. E., and Spindt, C. A., "100 W Operation of a Cold Cathode TWT," *IEEE Transactions on Electron Devices*, vol. 56, 2009, pp. 896–905.
[13] Child, C. D., "Discharge From Hot CaO," *Physical Review (Series I)*, vol. 32, May 1911, pp. 492–511.
[14] Langmuir, I., "The Effect of Space Charge and Residual Gases on Thermionic Currents in High Vacuum," *Physical Review*, vol. 2, Dec. 1913, pp. 450–486.
[15] Laframboise, J. G., and Sonmor, L. J., "Current collection by probes and electrodes in space magnetoplasmas: A review," *Journal of Geophysical Research: Space Physics*, vol. 98, 1993, pp. 337–357.
[16] Laframboise, J. G., and Parker, L. W., "Probe design for orbit-limited current collection," *Physics of Fluids*, vol. 16, May 1973, p. 629.
[17] Langmuir, I., and Blodgett, K. B., "Currents Limited by Space Charge between Concentric Spheres," *Physical Review*, vol. 24, Jul. 1924, pp. 49–59.
[18] Parker, L. W., and Murphy, B. L., "Potential buildup on an electron-emitting ionospheric satellite," *Journal of Geophysical Research*, vol. 72, 1967, pp. 1631–1636.
[19] Thompson, D. C., Bonifazi, C., Gilchrist, B. E., Williams, S. D., Raitt, W. J., Lebreton, J.-P., Burke, W. J., Stone, N. H., and Wright, K. H., "The current-voltage characteristics of a large probe in low Earth orbit: TSS-1R results," *Geophysical Research Letters*, vol. 25, 1998, pp. 413–416.
[20] Choiniere, E., and Gilchrist, B. E., "Self-Consistent 2-D Kinetic Simulations of High-Voltage Plasma Sheaths Surrounding Ion-Attracting Conductive Cylinders in Flowing Plasmas," *IEEE Transactions on Plasma Science*, vol. 35, 2007, pp. 7–22.
[21] Stone, N. H., Raitt, W. J., and Wright Jr., K. H., "The TSS-1R electrodynamic tether experiment: Scientific and technological results," *Advances in Space Research*, vol. 24, 1999, pp. 1037–1045.
[22] Cooke, D. L., and Katz, I., "TSS-1R electron currents: Magnetic limited collection from a heated presheath," *Geophysical Research Letters*, vol. 25, 1998, pp. 753–756.
[23] McTernan, J. K., and Bilen, S. G., "Electrodynamic Tether Systems on Small-Scale Spacecraft Using Dual-Purpose Materials for the Plasma-Spacecraft Interface," American Institute of Aeronautics and Astronautics, 2013.
[24] Conde, L., "An introduction to Langmuir probe diagnostics of plasmas" Available: http://plasmalab.aero.upm.es/~lcl/PlasmaProbes/Probes-2010-2.pdf.
[25] Bettinger, R. T., and Walker, E. H., "Relationship for Plasma Sheaths about Langmuir Probes," *Physics of Fluids*, vol. 8, Apr. 1965, p. 748.
[26] Barjatya, A., Swenson, C. M., Thompson, D. C., and Wright, K. H., "Invited Article: Data analysis of the Floating Potential Measurement Unit aboard the International Space Station," *Review of Scientific Instruments*, vol. 80, Apr. 2009, p. 041301.
[27] Rubin, B., Farnell, C., Williams, J., Vaughn, J., Schneider, T., and Ferguson, D., "Magnetic filter type plasma source for ground-based simulation of low earth orbit environment," *Plasma Sources Science and Technology*, vol. 18, May 2009, p. 025015.
[28] Bilén, S. G., n, Domonkos, M. T., and Gallimore, A. D., "Simulating Ionospheric Plasma with a Hollow Cathode in a Large Vacuum Chamber," *Journal of Spacecraft and Rockets*, vol. 38, Jul. 2001, pp. 617–621.
[29] Fujii, H., and Abe, T., "Current collection and discharges on high voltage solar array for space use in plasma," *IEEE Transactions on Plasma Science*, vol. 31, 2003, pp. 1001–1005.
[30] Chu, E., and Goebel, D. M., "High-Current Lanthanum Hexaboride Hollow Cathode for 10-to-50-kW Hall Thrusters," *IEEE Transactions on Plasma Science*, vol. 40, 2012, pp. 2133–2144.
[31] Trent, K. R., McDonald, M. S., Lobbia, R. B., and Gallimore, A. D., "Time-resolved Langmuir Probing of a New Lanthanum Hexaboride (LaB6) Hollow Cathode," *32nd International Electric Propulsion Conference*, Wiesbaden, Germany: 2011.
[32] Hastings, D., and Garrett, H. B., *Spacecraft--environment interactions*, Cambridge: Cambridge University Press, 2004.

[33] Goebel, D. M., Katz, and Wiley InterScience (Online service), *Fundamentals of electric propulsion ion and Hall thrusters*, Hoboken, N.J.: Wiley, 2008.
[34] Miller, J. S., Pullins, S. H., Levandier, D. J., Chiu, Y., and Dressler, R. A., "Xenon charge exchange cross sections for electrostatic thruster models," *Journal of Applied Physics*, vol. 91, Feb. 2002, p. 984.
[35] Sakabe, S., and Izawa, Y., "Cross sections for resonant charge transfer between atoms and their positive ions: Collision velocity ≲ 1 a.u.," *Atomic Data and Nuclear Data Tables*, vol. 49, Nov. 1991, pp. 257–314.
[36] "Francis F. Chen - Lecture Notes on Langmuir Probe Diagnostics," *Scribd* Available: http://www.scribd.com/doc/95164905/Francis-F-Chen-Lecture-Notes-on-Langmuir-Probe-Diagnostics.